

Lookahead Adversarial Semantic Segmentation

Hadi Jamali-Rad

Shell Global Solutions International B.V.

hadi.jamali-rad@shell.com

Attila Szabó*

University of Amsterdam (UvA)

attila.szabo@student.uva.nl

Matteo Presutto

Shell Global Solutions International B.V.

matteo.presutto@shell.com

Abstract

Semantic segmentation is one of the most fundamental problems in computer vision with significant impact on a wide variety of applications. Adversarial learning is shown to be an effective approach for improving semantic segmentation quality by enforcing higher-level pixel correlations and structural information. However, state-of-the-art semantic segmentation models cannot be easily plugged into an adversarial setting because they are not designed to accommodate convergence and stability issues in adversarial networks. We bridge this gap by building a conditional adversarial network with a state-of-the-art segmentation model (DeepLabv3+) at its core. To battle the stability issues, we introduce a novel lookahead adversarial learning approach (LoAd) with an embedded label map aggregation module. We demonstrate that the proposed solution can alleviate divergence issues in an adversarial semantic segmentation setting and results in considerable performance improvements (up to 5% in some classes) on the baseline for two standard datasets.¹

1 Introduction

Semantic segmentation is a challenging task in computer vision. It is a pivotal step towards content-based image analysis and scene understanding as it empowers machines to distinguish between different regions of an image based on its semantic context. To this aim, semantic segmentation models are trained to assign semantic labels to each and every pixel of an image as well as to cluster them into groups. Semantic segmentation has received an upsurge of attention recently owing to its wide variety of applications in medical imaging [1, 2], autonomous driving [3, 4], satellite image processing [5, 6], and robotics [7, 8], to name a few. Early segmentation methodologies are mostly developed with clustering algorithms at their core and somehow trying to incorporate contour, edge, and structural information. Examples of such algorithms are active contours [9], region-growing [10], conditional random fields (CRFs) [11], and sparse reconstruction based methods [12]. Recent advances in deep learning and convolutional neural networks (CNNs) revolutionized this field resulting in state-of-the-art image segmentation algorithms such as FCN [13], U-Net [1], PSPNet [14], EncNet [15], Exfuse [16], DeepLabv3+ [17], PS and Panoptic-DeepLab [18, 19], HRNet [20] and many other elegant architectures that considerably outperformed the traditional signal processing based methods addressing the same challenge.

*The work is done as part of an internship at Shell Global Solutions International B.V.

¹The code will be publicly released soon.

Majority of these deep learning based methods formulate semantic segmentation as a classification problem where cross entropy (CE) with pixel independence assumption is employed as the optimization loss function. However, in practice, adjacent pixels of an image are highly correlated. These methods implicitly assume that correlation among pixels would be learned as receptive field of CNNs increases going deeper with convolutions. Recent studies challenge this assumption and argue that overlooking pixel correlations explicitly can lead to performance degradation especially with regards to capturing structural information embedded in target classes. These studies have proposed different approaches to capture pixel inter-dependencies. For instance, CRFs can be used to model pixel relationships and enforce label consistency between pixels via similarity in visual appearance [21, 21, 22, 23]. However, CRFs are known to be time-consuming at inference and sensitive to variations in visual appearance. An alternative approach is extracting pixel affinity information from images and fusing them back to predicted label maps [24]; this comes at the cost of extra model branches and larger memory requirements. More recent studies have proposed changing the perspective and using different loss functions that encode the mutual information or structural similarity among nearby pixels in a regional fashion [25, 26] and have shown improvements. However, these losses can be derived in a sub-optimal manner by considering a small patch of pixels.

Another avenue that has been explored to enforce structure in segmentation is employing adversarial learning [27, 28, 29]. In this setup, a segmentor-discriminator pair compete to outperform each other in creating realistic label maps and distinguishing them from ground truth ones. We think a conditional adversarial approach similar to [27, 28] has the capacity to capture these pixel inter-dependencies and correlations in a more general (and not only local) fashion when compared to methods proposed in [25, 26]. On the other hand, plugging state-of-the-art semantic segmentation models in an adversarial setting is prone to the well-known divergence and mode collapse issues [30, 31]. Specific architecture designs for generator and discriminator networks can help to stabilize the setup, but at the cost of limiting the application domain of adversarial networks. When it comes to semantic segmentation, we are bound to architectures specifically designed to excel in doing so. When we tried to establish an adversarial network with DeepLabv3+ [17] as segmentor, we could not manage to stabilize the network regardless of remedies we pulled in. Bridging the gap between employing the state-of-the-art semantic segmentation models in adversarial settings and helping to stabilize them is the core idea of the proposed *lookahead adversarial* learning (LoAd) approach.

The proposed solution (LoAd) takes inspiration from the “lookahead optimizer” [32] and allows the semantic segmentation adversarial network to go ahead and actually diverge to some extent, then inspired by DAGGER in imitation learning [33] aggregates the degraded label maps, and steps backward to use these new sets of information and avoid further divergence. Notably, our label map aggregation is different from collecting adversarial examples to retrain and stabilize generative adversarial networks (GANs) [31, 34]. We demonstrate that LoAd can alleviate divergence issues of adversarial training in a semantic segmentation setting leading to improvement in mean-intersection-over-union (mIoU) over the baseline DeepLabv3+ on PASCAL VOC 2012 and Stanford Background datasets. We also show that in some classes 3% to 5% improvement in IoU beyond the baseline is achieved which is significant. We then qualitatively demonstrate that our solution is boosting the baseline in overall segmentation performance also in tackling class swap/confusion, and in understanding structure and continuity of the target classes.

2 Conditional Adversarial Training for Semantic Segmentation

Let $\mathcal{D}_t = \{(\mathbf{X}, \mathbf{Y})_1, \dots, (\mathbf{X}, \mathbf{Y})_M\}$ be the training dataset containing M samples with $\mathcal{X}_t = \{\mathbf{X} | (\mathbf{X}, \mathbf{Y}) \in \mathcal{D}_t\}$ and $\mathcal{Y}_t = \{\mathbf{Y} | (\mathbf{X}, \mathbf{Y}) \in \mathcal{D}_t\}$ respectively denoting the set of images and their corresponding label maps.² Here, \mathbf{X} is of size $H \times W \times 3$ for RGB images with a total of $H \times W = N$ pixels. The corresponding label map \mathbf{Y} is of size $H \times W$ with elements in $\mathcal{K} = \{1, \dots, K\}$ where K is the number of classes in the segmentation task.

²From now on, we use “map” and “label map” interchangeably.

An adaptation of conditional generative adversarial networks (CGANs) [35, 36, 37] for semantic segmentation would not require stochastic behavior in generating semantic label maps but aims at creating the most probable map \mathbf{Y} per input image \mathbf{X} . So, we solve a two-player min-max game to estimate $P(\mathbf{Y}|\mathbf{X})$

$$\min_G \max_D \mathcal{L}(G, D) = \mathbb{E}_{\mathbf{Y} \sim P_{\mathcal{D}_t}(\mathbf{Y})} [\log(D(\mathbf{Y}|\mathbf{X}))] + \mathbb{E}_{\mathbf{Y} \sim P_g(\mathbf{Y})} [\log(1 - D(\mathbf{Y}|\mathbf{X}))], \quad (1)$$

where $\mathcal{L}(\cdot)$ denotes the loss function, G denotes the generator (more specifically a segmentor) parameterized with θ_g , and D stands for the discriminator parameterized with θ_d . Typically, both G and D are CNN's. This can be further simplified within a binary classification setting where the discriminator is to decide whether a sample label map is ground truth ($\mathbf{Y} \sim P_{\mathcal{D}_t}$) or generated ($\mathbf{Y} \sim P_g$) by the segmentor. Considering binary cross entropy (CE), we arrive at the following adversarial loss

$$\mathcal{L}_a(\theta_g, \theta_d) = \sum_{m=1}^M [\log(D(\mathbf{Y}_m|\mathbf{X}_m)) + \log(1 - D(\hat{\mathbf{Y}}_m|\mathbf{X}_m))], \quad (2)$$

where $\hat{\mathbf{Y}}$ denotes the generated map. \mathcal{L}_a should be minimized w.r.t. θ_g and maximized w.r.t. θ_d . Several interesting studies such as [27, 28] suggest applying a hybrid loss combining the conditional adversarial loss in (2) with a regularization or CE pixel-wise term, sometimes in a slightly different context such as weakly supervised GAN settings [28]. The closest approach to our line of thought is the pioneering work in [27] where the following hybrid loss $\mathcal{L}_h = \mathcal{L}_p + \lambda \mathcal{L}_a$ is proposed

$$\mathcal{L}_h = \sum_{m=1}^M \text{CE}(\mathbf{Y}_m, \hat{\mathbf{Y}}_m) + \lambda \sum_{m=1}^M \log(D(\mathbf{Y}_m|\mathbf{X}_m)) + \lambda \sum_{m=1}^M \log(1 - D(\hat{\mathbf{Y}}_m|\mathbf{X}_m)), \quad (3)$$

where the pixel-wise loss \mathcal{L}_p is computed using a multi-class CE between the 1-hot encoded versions of the original label map \mathbf{Y} and the inferred one $\hat{\mathbf{Y}}$ using $-\sum_{i=1}^N \sum_{c=1}^K y_{i,c} \log(\hat{y}_{i,c})$, with y_i denoting the i th element of \mathbf{Y} . Obviously, only the second and the third terms in (3) are relevant when training the discriminator. When training the generator, [27] proposes to keep the first and the third terms. Next, a standard gradient decent ascent (GDA) [38] is applied to the two-player min-max game.

We decided to take a different approach for two reasons. First, interesting findings are recently reported in [39, 40] regarding the optimization of $\min_{x \in \mathbf{X}} \max_{y \in \mathbf{Y}} F(x, y)$ problems where $F(x, y)$ is concave in y and non-convex in x , which relates to our problem in that the loss is concave in θ_d and non-convex in θ_g in typical high dimensional settings with CNNs. Therefore, following the propositions in [39, 40], and (to our understanding) in contrast to [27], we avoid an alternating GDA in optimizing the generator and discriminator networks. Instead, in every "cycle" of the proposed adversarial approach (Algorithm 2), we keep training the discriminator with a dynamically updated dataset according to the proposed label map aggregation module (Algorithm 1) to reach sufficient accuracy before switching back to training the generator.

Second, based on our experience when incorporating state-of-the-art semantic segmentation models (like DeepLabv3+) in the adversarial setting, presence of the pixel-wise CE loss exacerbates the divergence issues. Therefore, another angle that distinguishes us from [27] is in how and when to incorporate the pixel-wise CE loss. We approach the problem in two stages as follows. Stage 1: if not pre-trained on \mathcal{D}_t , we first train the segmentation network using only CE pixel-wise loss up to a reasonable performance (without hard constraints). Stage 2: we then deactivate the pixel-wise CE loss (set it to 0) and run (LoAd) as described in Algorithm 2 to boost the performance. At this stage, when training discriminator both the second and the third terms of (3) will be active, and when training the segmentation network only the third term will be used where we follow the suggestion of [27, 35] and replace $+\lambda \sum_{m=1}^M \log(1 - D(\hat{\mathbf{Y}}_m|\mathbf{X}_m))$ with $-\lambda \sum_{m=1}^M \log(D(\hat{\mathbf{Y}}_m|\mathbf{X}_m))$ to maximize the probability of $\hat{\mathbf{Y}}_m$ being the true segmentation label map of \mathbf{X}_m .

3 Lookahead Adversarial Learning (LoAd)

The idea. Robustness and divergence issues of GANs are not secret to anyone [30, 31, 34, 41, 42]. Generally speaking, adversarial networks manifest the same difficulties and we had to tackle them in our semantic segmentation setup. Here is the idea behind lookahead adversarial learning (LoAd) for semantic segmentation in a nutshell. We take inspiration from “lookahead optimizer” [32] and allow the adversarial network to *go ahead* and actually diverge (to some extent) helping us to gain new insights and construct new datasets of label maps from these divergent (or degraded) models. Inspired by the idea of DAGGER [33], we aggregate these new datasets and use them for retraining the discriminator at the end of every cycle of LoAd. Next, we go back to where the divergence started (similar to “1 step back” in lookahead optimizer) to improve our next predictions and avoid further divergence. These new datasets are not designed or generated adversarial examples but sequentially degraded label maps. Note the importance of label maps in this context. When we descend towards divergence not only our performance metric goes down (mIoU, a single score) but also destructive impacts on the generated maps provides us with new sets of information that we exploit.

The mechanics. Algorithm 1 describes the map aggregation module of LoAd and Algorithm 2 provides a pseudo code level description of LoAd itself. Let us assume a starting model $g^s = g_0$ (e.g., the ending model after Stage 1 training as explained in Section 2). First, we evaluate the model on a subset of validation data (a hold-out set) to understand our current mIoU (denoted as μ in Algorithm 2). This serves as both starting and current best mIoU (μ^s and μ^* , respectively). We can already train our discriminator for the first time using $\mathcal{D}_t \cup g_0(\mathcal{X}_t)$, a set composed of full training data (images and maps) plus a set of generated (fake) maps. With this, we have initialized our label map aggregation buffer with $\mathcal{B} = \mathcal{B}[0] = g_0(\mathcal{X}_t)$ in Algorithm 1. Back to Algorithm 2, we then continue training adversarial until one of the following two criteria is met: a) patience iteration counter γ reaches its maximum Γ , alerting us that it is enough looking ahead, b) we diverge (in mIoU sense) reaching a pre-defined lower-bound ($\mu^s - \beta_l$) w.r.t. to the starting mIoU μ^s . If any of the two criteria are met, the cycle is finished, and we pick the last model of the cycle denoted by g^e . Throughout each cycle we also seek for an updated model offering a mIoU better than the starting one, and if such a new peak model g^* (above an upper-bound $\mu^s + \beta_u$) is found, the cycle would be returning two models, the best model of the cycle g^* besides its ending model g^e .

Per cycle one or both of these models $\{g^*, g^e\}$ would be passed to our map aggregation algorithm to generate new “fake” label maps which will be aggregated in \mathcal{B} . This dynamically updated dataset in \mathcal{B} concatenated with \mathcal{D}_t will then be used to retrain the discriminator before the next cycle starts. Owing to this label map aggregation and following retraining of the discriminator, we continually improve our adversarial model to avoid further divergences. At the end of each cycle, we go back and restart training adversarial from the newly found peak g^* or the old starting point g^s . Lastly, if we do more than Ψ cycles from a starting model g^s and a new peak is not found to replace it, the algorithm fully stops and returns the overall best model.

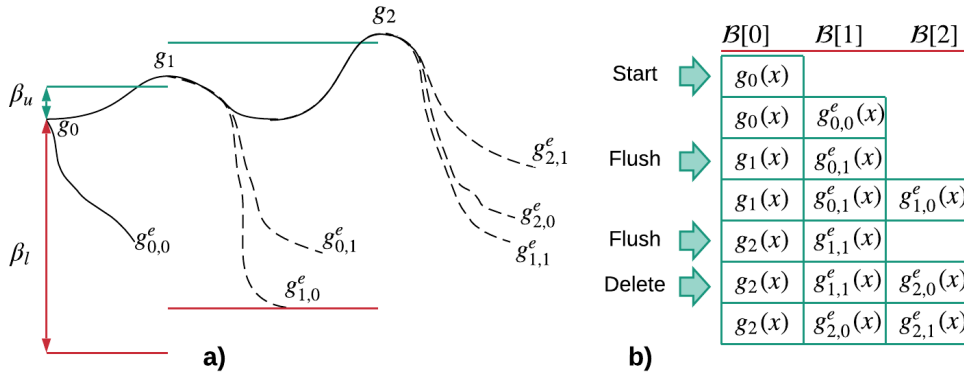


Figure 1: a) hypothetical convergence graph, b) corresponding label map aggregation buffer.

Algorithm 1: Map Aggregation Buffer

Require: peak/ending models, image set (g^p, g^e, \mathcal{X}) **if** $g^p \neq 0$ **then** Flush(\mathcal{B}) $\mathcal{B}[0] \leftarrow g^p(\mathcal{X})$ $\mathcal{B}[1] \leftarrow g^e(\mathcal{X})$ **else** **if** Size(\mathcal{B}) = max buffer size (B_{max}) **then** Delete($\mathcal{B}[1]$) **end** $\mathcal{B}[\text{end}] \leftarrow g^e(\mathcal{X})$ **end****Return:** \mathcal{B}

Algorithm 2: LoAd for Semantic Segmentation

Initialize: $\psi = 0$, $g^s = g_0$, $\mathcal{B} = g^s(\mathcal{X}_t)$ **Input:** maximum cycles: Ψ , maximum patience: Γ , β_l , β_u $\mu^s, \mu^*, \mu \leftarrow$ evaluate mIoUTrain Discriminator($\mathcal{D}_t \cup \mathcal{B}$)**while** $\psi < \Psi$ **do** start a divergence patience counter: $\gamma \leftarrow 0$ **while** $\mu^s - \beta_l < \mu$ and $\gamma < \Gamma$ **do** update model: $g \leftarrow$ Train Adversarial $\mu \leftarrow$ evaluate mIoU $\mu^* \leftarrow$ best $\mu > \mu^s + \beta_u$ update best model: $g^* \leftarrow g$ $\gamma \leftarrow \gamma + 1$ **end** $g^e \leftarrow$ keep the last model of the cycle **if** best model better than start **then** set best model as start model: $g^s \leftarrow g^*$ reset cycle counter $\psi \leftarrow 0$ $\mathcal{B} \leftarrow$ MapAggregation(g^*, g^e, \mathcal{X}) **else** $\mathcal{B} \leftarrow$ MapAggregation($0, g^e, \mathcal{X}$) start a new cycle $\psi \leftarrow \psi + 1$ **end** Train Discriminator($\mathcal{D}_t \cup \mathcal{B}$)**end**

Notably, the divergence patience counter γ is in practice updated in a dynamic manner (together with an auxiliary “peak finder” counter) to avoid an upward trend being stopped prematurely. Interested reader is referred to more details in the supplementary material.

The recap. To make this crystal clear, we use a hypothetical convergence graph in Fig. 1 a) and corresponding dynamically updated map aggregation buffer depicted in Fig. 1 b) to walk you through what LoAd does in action. As can be seen, starting from g_0 , the first adversarial cycle immediately descends towards divergence ending with $g_{0,0}^e$. We denote the j th cycle spawned from the i th peak with $g_{i,j}$. Note that $g_{0,0}^e$ does not descend by β_l , and thus, we are assuming that the cycle is ended due to reaching patience limit of Γ propagations (or

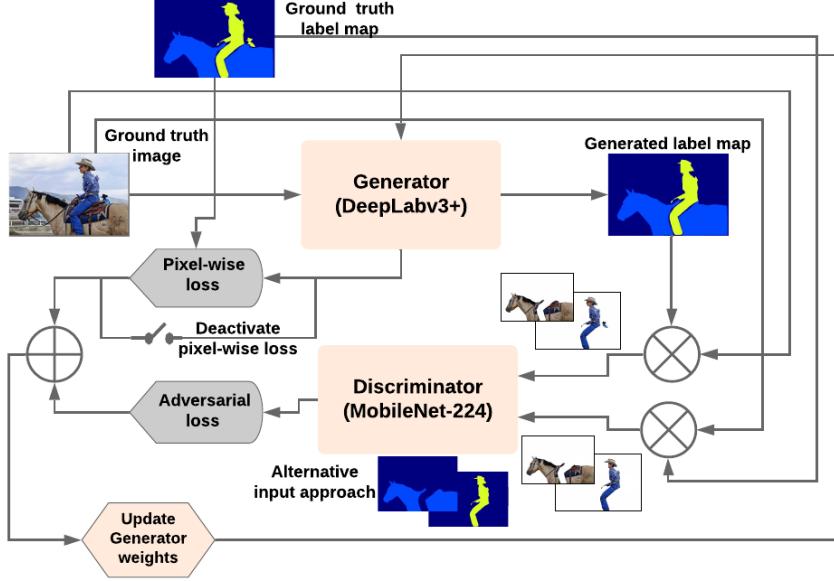


Figure 2: Adversarial network architecture.

iterations) as described in Algorithm 2. This cycle also did not introduce a new peak better than g_0 . Thus, only $g_{0,0}^e(\mathcal{X})$ will be added as a new set to the buffer \mathcal{B} . This is where we go back and restart adversarial training from g_0 , but this time with a retrained discriminator. As in the figure, this helps to ascend towards g_1 after which we diverge again in the second cycle. So, the second cycle returns a new peak $g^* = g_1$ as well as the ending model $g^e = g_{0,1}^e$ for map aggregation. Since a new peak is found (better than g^0), we **Flush** the buffer filling it with $\mathcal{B} = [g_1(\mathcal{X}) | g_{0,1}^e(\mathcal{X})]$ as shown in Fig. 1 b). Per pseudo code in Algorithm 1, any cycle that only returns an ending model (an no new peak) would result in creating a new label map set added to the end of the buffer unless the buffer is full; i.e., it already contains B_{max} label map sets. In that case, we first **Delete** the label map set corresponding to the oldest ending model and then the new label map set is added to the end of \mathcal{B} . An example of this scenario in our hypothetical setup is where the set corresponding to $g_{1,1}^e$ is deleted in favor of the newcomer set corresponding to $g_{2,1}^e$.

4 Experimental Setup

Network architecture. Our experimental network architecture is shown in Fig. 2. As can be seen, we opted for DeepLabv3+ with a modified Xception-65 backbone [17], bearing in mind that DeepLabv3+ might not be the easiest model to simply plug into an adversarial settings. We chose Mobilenet-224 [43] as our discriminator. The figure shows our discriminator training policy being conditional on the input image split into different classes (using ground truth and generated label maps) and stacked into the input channels of the discriminator. We also considered a few other possibilities such as feeding the discriminator with split label maps themselves, which did not result in improvement. To connect the discriminator and generator, we used Gumbel softmax with temperature parameter $\tau = 20$ [44]. Our trainings are run separately on Nvidia P100 Tesla nodes each with 16 GB of memory. Notably, we are particularly interested in models that *run fast at inference* time for *near real-time* field applications. That is why we picked a DeepLabv3+ base model that offers speed (no multi-scaling, no CRFs) and performance at the same time.

Adversarial training. Per cycle in Algorithm 2, we train MobileNet (discriminator) until sufficient performance is reached using an early-stopping criterion on the validation loss evaluated on the hold-out set.

We used a batch size of 16, and set $\alpha = 1$ with a dropout rate of 0.01 [43]. We used Adagrad as optimizer with a learning rate of $lr_d = 0.01$. Because of the label map aggregation, the loss function of the discriminator (binary CE) is weighted to account for the variable number of generated label maps in the map aggregation buffer. For adversarial training, we used a batch size of 5 due to the memory limitation of the GPU nodes available. The adversarial learning rate was set to $lr_a = 2.5e - 7$, and we trained using a momentum of 0.95. Bear in mind that the temperature parameter $\tau = 20$ in effect boosts the lr_a . Adversarial training is conducted based on LoAd (in Algorithm 2) with $\beta_u = 0.001$ corresponding to 0.1% improvement in mIoU and $\beta_l = 0.05$ corresponding to 5% drop in mIoU in a cycle. Patience counter maximum is set to $\Gamma = 20$, and maximum number of cycles allowed is set to $\Psi = 50$. Maximum buffer set size is $B_{max} = 3$.

PASCAL VOC 2012 dataset. PASCAL VOC 2012 dataset [45] contains 20 foreground object classes and 1 background class. It contains 1,464 train, 1,449 validation, and 1,456 test pixel-level annotated images. For the experiments on this dataset, we started from DeepLabv3+ checkpoint pre-trained on PASCAL VOC 2012 achieving mIoU = 82.2% (see, Table 5 in [17]) followed by applying LoAd without any further fine-tuning. Since the images have a shape of at most 512×512 pixels, we used a crop size of 513×513 for DeepLabv3+ input layer following the recommendations in [17]. For early stopping evaluation when training the discriminator as well as for evaluating the mIoU during adversarial training we used 30% (500 images) of the validation set (as hold-out set).

Stanford Background dataset. The Stanford Background dataset [46] contains 8 classes of scene elements. It has 715 pixel-level annotated images which we have split into 400 for training, 172 for validation (hold-out) and 143 for testing. For this dataset, there was no pre-trained DeepLabv3+ model available and we followed our two stage approach as explained in Section 2. We used DeepLabv3+ checkpoint from Cityscapes achieving mIoU of 78.79% (see Table 7 in [17]) and trained it on Stanford Background using only pixel-wise CE loss. We set batch size to 7 and trained the model with a weighted CE loss for 4 epochs then switched to the original CE loss (all weights set to 1) and trained for another 8 epochs reaching mIoU = 74.33%. Weighted CE loss is calculated by multiplying the loss by the average number of pixels per class computed over the entire training dataset and dividing it by the number of pixel per class in the image. This model is then used as the starting point for applying and evaluating LoAd. The learning rate for the pixel-wise training was set to $lr_p = 0.0001$ and kept constant throughout the training following [17]. We did not use multi-scale training policies for DeepLabv3+, and followed the recommendations of [17] to upscale the logits to input image size for evaluation. Pictures in the Stanford Background dataset have a maximum pixel size of 320×320 for which we used 321×321 as crop size as suggested in [17].

Augmentation, inference, and evaluation. We augmented the pictures with random flips for both pixel-wise and adversarial training stages. Both Stanford Background and PASCAL VOC 2012 have “ignored” (unlabeled) pixel class in the ground truth annotation label maps but the generated label maps do not. We handled this by relabeling the ignored pixels to “background” class in both ground truths and generated label maps. At inference time, we used original images as input to the models, and no special inference strategy is applied. The evaluation metric is the mIoU score.

5 Evaluation Results

Results on PASCAL VOC 2012. Fig. 3 shows the convergence graph evaluated on the hold-out set. Note the behavioral similarity to the sketch presented in Fig.1 a). As can be seen, starting from the baseline DeepLabv3+ with mIoU= 82.2% (denoted by g_0), we initially diverge towards $g_{0,0}$ and $g_{0,1}$ in the first and second cycles, each time applying map aggregation as discussed in Section 3. This clearly helped to stabilize the model in the third cycle to ascend from g_0 towards g_1 as the new peak along the path and ending with $g_{0,2}$. This process is continued following the mechanics of LoAd as described in Section 3 alleviating the unstable behavior of the adversarial network helping it to sequentially improve. Table 1 summarizes the

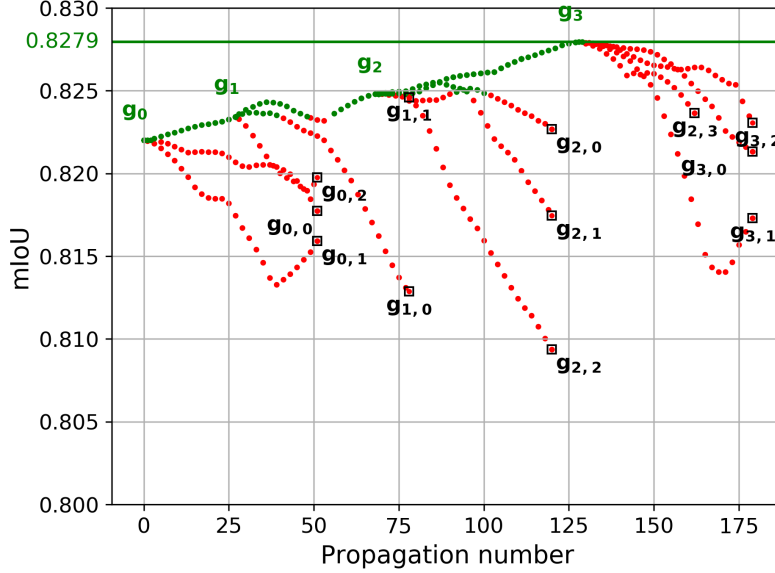


Figure 3: Convergence graph of PASCAL VOC 2012.

Table 1: Performance comparison on PASCAL VOC 2012 *validation* set.

Method	backg.	aero.	bicycle	bird	boat	bottle	bus	car	cat	chair	cow
DeepLabv3+	95.55	90.33	44.23	89.56	72.15	81.11	96.76	91.37	94.33	51.87	96.08
DLv3+ & LoAd	95.65	92.92	43.86	90.31	77.73	82.02	96.29	90.18	94.20	51.73	95.55
contd.	d.table	dog	horse	m.bike	person	p.plant	sheep	sofa	train	tv	mIoU
DeepLabv3+	60.14	92.63	93.33	89.23	90.18	67.19	93.75	61.26	94.81	80.27	82.20
DLv3+ & LoAd	64.28	92.14	93.30	88.63	90.19	67.65	93.65	64.93	94.18	80.31	82.84

performance comparison between the baseline (DeepLabv3+, also denoted as DLv3+ for brevity) and the proposed boosted model after applying LoAd (DeepLabv3+ & LoAd) on the full validation set. The results are interesting in the sense that even though the overall mIoU has increased by 0.6%, in some of the highlighted classes such as “aeroplane”, “sofa”, “diningtable”, and “boat” the improvement in IoU ranges from +2% to +5% which is quite significant. Obviously, we degrade in some other classes mostly by a fraction of a percent, except for the “car” class where we degrade by more than 1%. To further consolidate our understanding, we also submitted the results of the baseline DeepLabv3+ and LoAd on the test data of PASCAL VOC 2012 to its evaluation server. The outcome in Table 2 once again corroborates our claim. The overall mIoU improvement stays about 0.6% over the baseline, with even a larger number of classes outperforming the baseline when compared to the validation set. On the contrary, less extreme performance jumps can be observed (maximum of about 3%). Check out the anonymized results for the baseline DeepLabv3+³ and the proposed method⁴ on PASCAL VOC server.

A selected set of qualitative results are illustrated in Fig 4. On the top row, the whole dining table is missed by the baseline model and LoAd manages to boost DeepLabv3+ to fully recover that. “Bird” tails are interesting example of how discontinuity is less of an impediment for the proposed method. On the third row, once again the impact is significant, a misconception of “boat” in the middle of water is resolved. On the same note, fourth row depicts cleaner edges. Last two rows show interesting signs of avoiding class swap/confusion. Being a rather difficult case to distinguish even for human observer, LoAd helps DeepLabv3+ to resolve mistaking

³DeepLabv3+: <http://host.robots.ox.ac.uk:8080/anonymous/SPNVZZ.html>

⁴DeepLabv3+&LoAd: <http://host.robots.ox.ac.uk:8080/anonymous/OCEIMG.html>

Table 2: Performance comparison on PASCAL VOC 2012 *test* set.

Method	backg.	aero.	bicycle	bird	boat	bottle	bus	car	cat	chair	cow
DeepLabv3+	93.52	84.27	39.70	86.22	66.67	79.68	92.12	81.89	85.84	42.40	82.91
DLv3+ & LoAd	93.63	84.69	39.52	86.42	68.14	79.31	92.24	85.07	85.87	43.79	82.41
contd.	d.table	dog	horse	m.bike	person	p.plant	sheep	sofa	train	tv	mIoU
DeepLabv3+	75.20	84.10	83.64	86.17	82.68	62.54	81.69	63.39	81.60	76.70	76.81
DLv3+ & LoAd	77.07	84.23	83.80	85.88	82.69	62.05	81.70	65.79	83.40	77.41	77.39

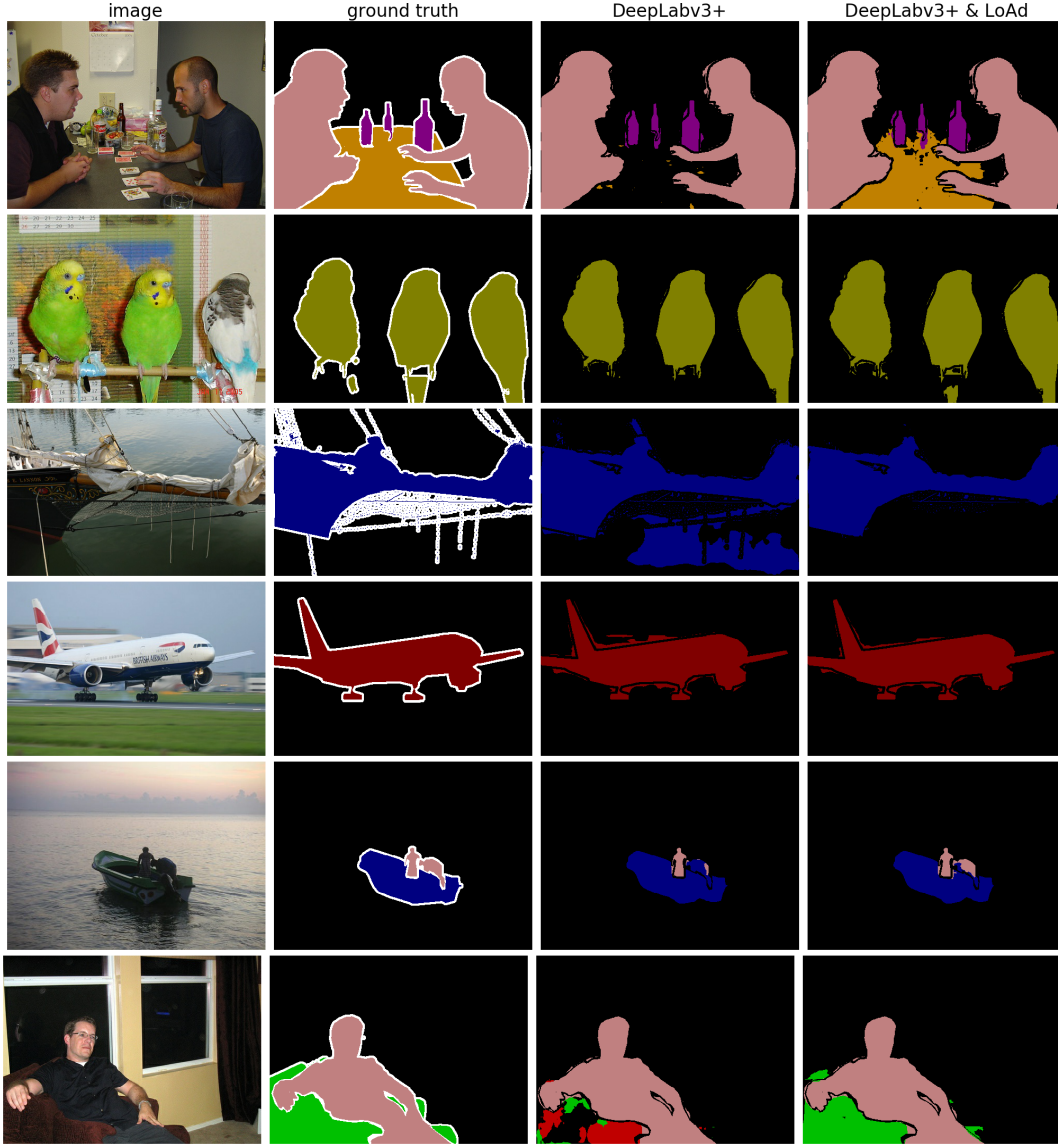


Figure 4: Selected qualitative results on PASCAL VOC 2012 validation set. Interesting examples show how totally missing items (dining table, first row), discontinuity (bird tail, second row), inconsistent body/edges (third and fourth rows) and class swap and confusion (last two rows) are resolved or considerably improved. Best view in color with 300% zoom.

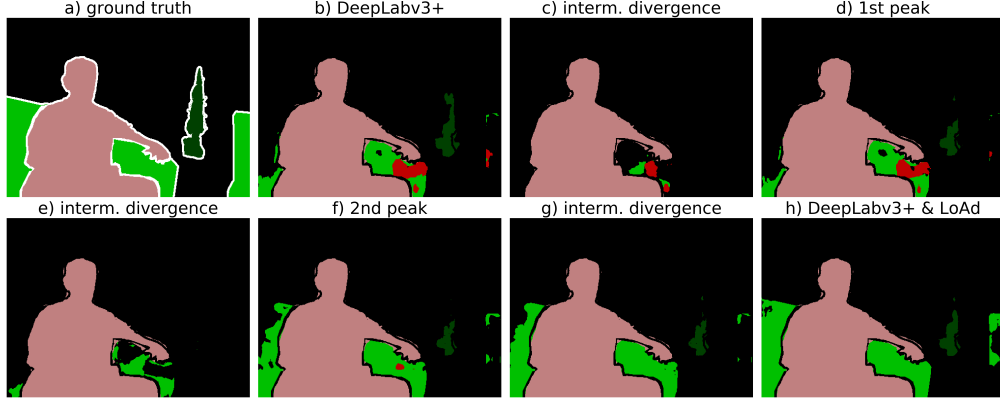


Figure 5: This illustrates how LoAd benefits from map aggregation throughout its convergence process to not only resolve class confusion of baseline DeepLabv3+ in b) (g_0 in Fig 2) but also gradually in d), f) and h) (g_1 , g_2 and g_3) build up towards a more consistent understanding of “sofa”.

Table 3: Performance comparison on Stanford Background *test* set.

Method	sky	tree	road	grass	water	building	mountain	foreground	mIoU
DeepLabv3+	89.38	72.21	87.28	77.44	72.70	80.03	48.64	66.92	74.33
DeepLabv3+ & LoAd	89.47	72.89	87.71	77.90	73.89	80.87	50.11	67.54	75.05

the second “person” on the boat with boat engine. The same can be argued about the last row in which “sofa” vs. “chair” confusion is resolved. Fig 5 shows yet another example from the validation set with considerable improvement. Here, we would like to accentuate on the gradual impact of LoAd with its embedded dynamic map aggregation. As can be seen, starting from the baseline DeepLabv3+, LoAd gradually learns from the intermediate degradation in its downward divergent stages at c), e) and g) and resolves confusion with “chair” (red pixels) as well as manages to also detect the second instance of sofa in the image which is missed by the baseline DeepLabv3+. Several other examples are provided in the supplementary materials.

Results on Stanford Background. To further investigate the impact of the proposed approach, we also evaluated LoAd on Stanford Background dataset. We chose this dataset for three reasons: 1) to explore what the impact on smaller datasets (from sample size perspective) would be, 2) to try somewhat different type of classes (scene elements vs. objects in PASCAL VOC 2012), and 3) to expedite the training due to overall smaller image sizes. The results are summarized in Table 3. As can be seen, applying LoAd on DeepLabv3+ boosts the overall mIoU by 0.7% (slightly more than PASCAL VOC 2012), and this time it consistently outperform the baseline on all classes without any exception with considerable improvement on two classes (“mountain” and “water”).

6 Concluding Remarks

Summary and impact. We proposed a novel lookahead adversarial learning (LoAd) approach with an embedded label map aggregation idea for adversarial semantic segmentation with state-of-the-art models. For experimental evaluation, we picked DeepLabv3+ as segmentor/generator in the adversarial setting. We further elaborated in Section 4 that among a few available choices for DeepLabv3+ (also abbreviated as DLv3+) architectures and corresponding training/inference strategies, we deliberately picked one which *runs fast at inference time* (0.7 sec on average per sample input image). Therefore, we did not opt for models requiring multi-scaling strategies or small output strides leading to several minutes or in some cases few tens of minutes inference time per image. Running fast at inference time for field applications is a *core motive* of this work. We demonstrated that the proposed idea can moderately improve the performance of the baseline DeepLabv3+ in mIoU sense while boosting the performance of certain classes up to 5% without introducing any extra delay at inference time; it runs practically as fast as the baseline on top of which it is applied. The qualitative results show that our approach is helping the baseline segmentation model to resolve class confusion to a good extent as well as to produce label maps which are more consistent in terms of continuity and structure. We think the application domain of LoAd could possibly be larger than semantic segmentation. This is an interesting avenue to explore.

Complexity. LoAd adds architectural complexity by adding a (simple) discriminator network but requires no changes to the base segmentation model, as such in theory, it can be applied on top of any semantic segmentation model (not only DeepLabv3+). On the flip side, we introduce complexity at training both in time and space slowing it down in favor of performance. Roughly speaking, in worst case scenario of large size images containing N pixels, for an evaluation (hold-out) subset of size V_e samples, we impose an extra $\mathcal{O}(V_e N)$ time complexity per propagation for adversarial training. In practice, $V_e \ll N$. Also, with the label map aggregation module of LoAd we need to train the discriminator on $B_{\max} M$ images stacked in the buffer (space complexity) instead of only M_b images in a batch with $M_b \ll M$. On the other hand, we train the discriminator once per LoAd cycle, i.e., orders of magnitude less often than typical GDA based adversarial training. One way to lessen this complexity is to train the discriminator with a portion of the training data, for instance, with images seen up to that moment in training. That can already be accommodated in Algorithm 1 without any modification.

Future directions. We are currently working on replacing DeepLabv3+ with another state-of-the-art segmentation network and analyzing the impact. So far, we have understood that slightly different map aggregation policies can be beneficial in different architectures. As an example, one could replace the **Flush** operation that cleans up all the previous aggregated maps with **Retain** for which always a certain number of previous peaks (from previous cycles) are retained. In the supplementary material, we already take one step towards this ablation study direction by changing the backbone of DeepLabv3+. Obviously, a more general understanding of the impact of LoAd requires it to be applied to other applications beyond semantic segmentation which is outside the scope of this work.

Acknowledgment

The authors are thankful to Ahmad Zamanian for helpful discussions on adversarial networks, and to Saptarshi Das, Jose Gonzalez Martinez, Daniel Jeavons, and other members of Shell Global Solutions International B.V. for their support. Hadi Jamali-Rad is thankful to Ahmad Beirami from Facebook AI for pointers to DAGGER [33] and sharing insights on the results reported in [39, 40].

References

- [1] O. Ronneberger, P. Fischer, and T. Brox, “U-Net: Convolutional networks for biomedical image segmentation,” in *International Conference on Medical image computing and computer-assisted intervention*, pp. 234–241, Springer, 2015.
- [2] M. Rezaei, K. Harmuth, W. Gierke, T. Kellermeier, M. Fischer, H. Yang, and C. Meinel, “A conditional adversarial network for semantic segmentation of brain tumor,” in *International MICCAI Brainlesion Workshop*, pp. 241–252, Springer, 2017.
- [3] M. Menze and A. Geiger, “Object scene flow for autonomous vehicles,” in *Proceedings of the IEEE conference on computer vision and pattern recognition (CVPR)*, pp. 3061–3070, 2015.
- [4] M. Cordts, M. Omran, S. Ramos, T. Rehfeld, M. Enzweiler, R. Benenson, U. Franke, S. Roth, and B. Schiele, “The cityscapes dataset for semantic urban scene understanding,” in *Proceedings of the IEEE conference on computer vision and pattern recognition (CVPR)*, pp. 3213–3223, 2016.
- [5] M. Volpi and V. Ferrari, “Semantic segmentation of urban scenes by learning local class interactions,” in *Proceedings of the IEEE Conference on Computer Vision and Pattern Recognition (CVPR) Workshops*, pp. 1–9, 2015.
- [6] C. Henry, S. M. Azimi, and N. Merkle, “Road segmentation in sar satellite images with deep fully convolutional neural networks,” *IEEE Geoscience and Remote Sensing Letters*, vol. 15, no. 12, pp. 1867–1871, 2018.
- [7] A. Geiger, P. Lenz, C. Stiller, and R. Urtasun, “Vision meets robotics: The kitti dataset,” *The International Journal of Robotics Research*, vol. 32, no. 11, pp. 1231–1237, 2013.
- [8] A. A. Shvets, A. Rakhlin, A. A. Kalinin, and V. I. Iglovikov, “Automatic instrument segmentation in robot-assisted surgery using deep learning,” in *2018 17th IEEE International Conference on Machine Learning and Applications (ICMLA)*, pp. 624–628, IEEE, 2018.
- [9] M. Kass, A. Witkin, and D. Terzopoulos, “Snakes: Active contour models,” *International journal of Computer Vision*, vol. 1, no. 4, pp. 321–331, 1988.
- [10] R. Nock and F. Nielsen, “Statistical region merging,” *IEEE Transactions on pattern analysis and machine intelligence*, vol. 26, no. 11, pp. 1452–1458, 2004.
- [11] N. Plath, M. Toussaint, and S. Nakajima, “Multi-class image segmentation using conditional random fields and global classification,” in *Proceedings of the 26th Annual International Conference on Machine Learning (ICML)*, pp. 817–824, 2009.
- [12] S. Minaee and Y. Wang, “An ADMM approach to masked signal decomposition using subspace representation,” *IEEE Transactions on Image Processing*, vol. 28, no. 7, pp. 3192–3204, 2019.
- [13] J. Long, E. Shelhamer, and T. Darrell, “Fully convolutional networks for semantic segmentation,” in *Proceedings of the IEEE conference on computer vision and pattern recognition (CVPR)*, pp. 3431–3440, 2015.
- [14] H. Zhao, J. Shi, X. Qi, X. Wang, and J. Jia, “Pyramid scene parsing network,” in *Proceedings of the IEEE conference on computer vision and pattern recognition (CVPR)*, pp. 2881–2890, 2017.
- [15] H. Zhang, K. Dana, J. Shi, Z. Zhang, X. Wang, A. Tyagi, and A. Agrawal, “Context encoding for semantic segmentation,” in *Proceedings of the IEEE conference on Computer Vision and Pattern Recognition*, pp. 7151–7160, 2018.
- [16] Z. Zhang, X. Zhang, C. Peng, X. Xue, and J. Sun, “Exfuse: Enhancing feature fusion for semantic segmentation,” in *Proceedings of the European Conference on Computer Vision (ECCV)*, pp. 269–284, 2018.
- [17] L.-C. Chen, Y. Zhu, G. Papandreou, F. Schroff, and H. Adam, “Encoder-decoder with atrous separable convolution for semantic image segmentation,” in *Proceedings of the European conference on computer vision (ECCV)*, pp. 801–818, 2018.
- [18] A. Kirillov, K. He, R. Girshick, C. Rother, and P. Dollár, “Panoptic segmentation,” in *Proceedings of the IEEE conference on computer vision and pattern recognition*, pp. 9404–9413, 2019.

- [19] B. Cheng, M. D. Collins, Y. Zhu, T. Liu, T. S. Huang, H. Adam, and L.-C. Chen, “Panoptic-deeplab,” *arXiv preprint arXiv:1910.04751*, 2019.
- [20] J. Wang, K. Sun, T. Cheng, B. Jiang, C. Deng, Y. Zhao, D. Liu, Y. Mu, M. Tan, X. Wang, *et al.*, “Deep high-resolution representation learning for visual recognition,” *IEEE transactions on pattern analysis and machine intelligence*, 2020.
- [21] Z. Liu, X. Li, P. Luo, C. C. Loy, and X. Tang, “Deep learning markov random field for semantic segmentation,” *IEEE transactions on pattern analysis and machine intelligence*, vol. 40, no. 8, pp. 1814–1828, 2017.
- [22] L.-C. Chen, G. Papandreou, I. Kokkinos, K. Murphy, and A. L. Yuille, “Deeplab: Semantic image segmentation with deep convolutional nets, atrous convolution, and fully connected crfs,” *IEEE transactions on pattern analysis and machine intelligence*, vol. 40, no. 4, pp. 834–848, 2017.
- [23] F. Shen, R. Gan, S. Yan, and G. Zeng, “Semantic segmentation via structured patch prediction, context crf and guidance crf,” in *Proceedings of the IEEE Conference on Computer Vision and Pattern Recognition*, pp. 1953–1961, 2017.
- [24] T.-W. Ke, J.-J. Hwang, Z. Liu, and S. X. Yu, “Adaptive affinity fields for semantic segmentation,” in *Proceedings of the European Conference on Computer Vision (ECCV)*, pp. 587–602, 2018.
- [25] S. Zhao, Y. Wang, Z. Yang, and D. Cai, “Region mutual information loss for semantic segmentation,” in *Advances in Neural Information Processing Systems*, pp. 11115–11125, 2019.
- [26] S. Zhao, B. Wu, W. Chu, Y. Hu, and D. Cai, “Correlation maximized structural similarity loss for semantic segmentation,” *arXiv preprint arXiv:1910.08711*, 2019.
- [27] P. Luc, C. Couprie, S. Chintala, and J. Verbeek, “Semantic segmentation using adversarial networks,” *arXiv preprint arXiv:1611.08408*, 2016.
- [28] N. Souly, C. Spampinato, and M. Shah, “Semi supervised semantic segmentation using generative adversarial network,” in *Proceedings of the IEEE International Conference on Computer Vision*, pp. 5688–5696, 2017.
- [29] Y. Xue, T. Xu, H. Zhang, L. R. Long, and X. Huang, “SegAN: Adversarial network with multi-scale L1 loss for medical image segmentation,” *Neuroinformatics*, vol. 16, no. 3-4, pp. 383–392, 2018.
- [30] M. Arjovsky, S. Chintala, and L. Bottou, “Wasserstein gan,” *arXiv preprint arXiv:1701.07875*, 2017.
- [31] I. J. Goodfellow, J. Shlens, and C. Szegedy, “Explaining and harnessing adversarial examples,” *arXiv preprint arXiv:1412.6572*, 2014.
- [32] M. Zhang, J. Lucas, J. Ba, and G. E. Hinton, “Lookahead optimizer: k steps forward, 1 step back,” in *Advances in Neural Information Processing Systems*, pp. 9593–9604, 2019.
- [33] S. Ross, G. Gordon, and D. Bagnell, “A reduction of imitation learning and structured prediction to no-regret online learning,” in *Proceedings of the fourteenth international conference on artificial intelligence and statistics*, pp. 627–635, 2011.
- [34] X. Liu and C.-J. Hsieh, “Rob-GAN: Generator, discriminator, and adversarial attacker,” in *Proceedings of the IEEE Conference on Computer Vision and Pattern Recognition*, pp. 11234–11243, 2019.
- [35] I. Goodfellow, J. Pouget-Abadie, M. Mirza, B. Xu, D. Warde-Farley, S. Ozair, A. Courville, and Y. Bengio, “Generative adversarial nets,” in *Advances in neural information processing systems*, pp. 2672–2680, 2014.
- [36] M. Mirza and S. Osindero, “Conditional generative adversarial nets,” *arXiv preprint arXiv:1411.1784*, 2014.
- [37] P. Isola, J.-Y. Zhu, T. Zhou, and A. A. Efros, “Image-to-image translation with conditional adversarial networks,” in *Proceedings of the IEEE conference on computer vision and pattern recognition*, pp. 1125–1134, 2017.
- [38] T. Lin, C. Jin, and M. I. Jordan, “On gradient descent ascent for nonconvex-concave minimax problems,” *arXiv preprint arXiv:1906.00331*, 2019.

- [39] M. Nouiehed, M. Sanjabi, T. Huang, J. D. Lee, and M. Razaviyayn, “Solving a class of non-convex min-max games using iterative first order methods,” in *Advances in Neural Information Processing Systems*, pp. 14905–14916, 2019.
- [40] D. M. Ostrovskii, A. Lowy, and M. Razaviyayn, “Efficient search of first-order nash equilibria in nonconvex-concave smooth min-max problems,” *arXiv preprint arXiv:2002.07919*, 2020.
- [41] K. Roth, A. Lucchi, S. Nowozin, and T. Hofmann, “Stabilizing training of generative adversarial networks through regularization,” in *Advances in neural information processing systems*, pp. 2018–2028, 2017.
- [42] T. Salimans, I. Goodfellow, W. Zaremba, V. Cheung, A. Radford, and X. Chen, “Improved techniques for training gans,” in *Advances in neural information processing systems*, pp. 2234–2242, 2016.
- [43] A. G. Howard, M. Zhu, B. Chen, D. Kalenichenko, W. Wang, T. Weyand, M. Andreetto, and H. Adam, “Mobilenets: Efficient convolutional neural networks for mobile vision applications,” *arXiv preprint arXiv:1704.04861*, 2017.
- [44] E. Jang, S. Gu, and B. Poole, “Categorical reparameterization with gumbel-softmax,” *arXiv preprint arXiv:1611.01144*, 2016.
- [45] M. Everingham, S. A. Eslami, L. Van Gool, C. K. Williams, J. Winn, and A. Zisserman, “The pascal visual object classes challenge: A retrospective,” *International journal of computer vision*, vol. 111, no. 1, pp. 98–136, 2015.
- [46] S. Gould, R. Fulton, and D. Koller, “Decomposing a scene into geometric and semantically consistent regions,” in *2009 IEEE 12th international conference on computer vision*, pp. 1–8, IEEE, 2009.

A Lookahead Adversarial Semantic Segmentation: Supplementary Material

In the following, we provide further evidence on the impact of the proposed approach. After a brief note on the limitations of pixel-wise cross-entropy (CE) loss, we dive deep into the mechanics of LoAd providing an extended and more detailed version of Algorithm 2 besides a process flowchart view of the proposed method. We then present some ablation studies in which we analyze the impact of changing the backbone of DeepLabv3+ (from Xception-65 to MobileNetv2) as well as investigate the influence of varying two selected hyperparameters of LoAd. Finally, we provide further qualitative results on the impact of the proposed method. **Remark:** please note that PASCAL VOC server can be slow sometimes and might require refreshing the page a few times.

B On the Dimensionality of the Problem

Let us briefly reflect on why employing only a pixel-wise cross-entropy (CE) optimization loss for semantic segmentation and relying on gradual increase in receptive field of CNNs might not be sufficient for explicitly promoting a large set of candidate solutions for label maps. A good portion of these solutions might not be valid, bearing in mind that missing out on the rest could also lead to sub-optimal solutions for the segmentation problem. This is in line with literature [21, 21, 22, 23, 24, 25, 26] proposing different approaches to address this challenge. Following our notation in Section 2, let $\mathcal{D}_t = \{(\mathbf{X}, \mathbf{Y})_1, \dots, (\mathbf{X}, \mathbf{Y})_M\}$ be training dataset with M samples so that for all $(\mathbf{X}, \mathbf{Y})_i \in \mathcal{D}_t$, $(\mathbf{X}, \mathbf{Y})_i \sim P(\mathbf{X}, \mathbf{Y})$ where $\mathcal{X}_t = \{\mathbf{X} | (\mathbf{X}, \mathbf{Y}) \in \mathcal{D}_t\}$ and $\mathcal{Y}_t = \{\mathbf{Y} | (\mathbf{X}, \mathbf{Y}) \in \mathcal{D}_t\}$ respectively denote the set of images and their corresponding label maps in the training dataset. As discussed earlier, \mathbf{X} is of size $H \times W \times 3$ for RGB images with a total of N pixels and the corresponding label map \mathbf{Y} is of size $H \times W$ with elements in $\mathcal{K} = \{1, \dots, K\}$ where K is the number of classes in segmentation task. Let $P(\mathbf{X})$, $P(\mathbf{Y})$ and $P(\mathbf{X}, \mathbf{Y})$ denote probability mass functions of corresponding categorical distributions. Now, with pixel independence assumption:

$$P(\mathbf{Y}) = \prod_{i=1}^N P(y_i), \quad (4)$$

where y_i denotes the i th pixel in \mathbf{Y} . This obviously ignores the potential correlation among the pixels. $P(\mathbf{Y})$ is a function from the set $E_{\mathbf{Y}}$, comprised of all possible values \mathbf{Y} can take, to a probability in \mathbb{R} . As such, learning $P(\mathbf{Y})$ mandates exploring $E_{\mathbf{Y}} \times \mathbb{R}$. But how do all possible maps in $E_{\mathbf{Y}}$ look like? To answer this, let us consider a toy setup where \mathbf{Y} is a 2×1 label map $\begin{bmatrix} y_1 \\ y_2 \end{bmatrix}$ with $K = 3$ classes in $\mathcal{K} = \{1, 2, 3\}$. The set of all possible label maps is simply:

$$E_{\mathbf{Y}} = \left\{ \begin{bmatrix} 1 \\ 1 \end{bmatrix}, \begin{bmatrix} 2 \\ 1 \end{bmatrix}, \begin{bmatrix} 3 \\ 1 \end{bmatrix}, \begin{bmatrix} 1 \\ 2 \end{bmatrix}, \begin{bmatrix} 2 \\ 2 \end{bmatrix}, \begin{bmatrix} 3 \\ 2 \end{bmatrix}, \begin{bmatrix} 1 \\ 3 \end{bmatrix}, \begin{bmatrix} 2 \\ 3 \end{bmatrix}, \begin{bmatrix} 3 \\ 3 \end{bmatrix} \right\},$$

whose size is equal to the permutations with replacement of 2 pixels from a set of 3 classes, i.e., $3^2 = 9$. One can straightforwardly generalize this toy example to any arbitrary number of pixels N and classes K and show that $|E_{\mathbf{Y}}| = K^N$ where $|\mathcal{A}|$ denotes the cardinality of set \mathcal{A} . Following the same approach, this time with pixel independence assumption in (4) for y_1 and y_2 , the set of permutations would be 6, counting 3 possible values per y_i summing them up due to independence. Again, it is straightforward to show $|E_{\mathbf{Y}}| = KN$. This toy example illustrates how the solution space of the problem with pixel independence assumption is significantly smaller than the one considering all possible correlations between pixels. However, the latter can easily become intractable for large size images, and that is the reason why a pixel-wise loss has been so popular. We think a conditional adversarial approach has the capacity to partially explore the larger solution space and to capture these pixel correlations in a general (and not only local) fashion.

C Deeper Dive in Lookahead Adversarial Learning (LoAd)

As discussed in Section 3, there are subtle details we skipped or described on a high level to convey the core idea of the proposed method (LoAd) and not to steal the readers attention away from the main message. In this section, we dive deeper into the mechanics of LoAd using Fig. 6, a flow chart that breaks down its process flow in clear terms, together with a more detailed version of Algorithm 2. For the sake of clarity, we are using line numbers in Algorithm 3 to be able to refer to specific lines throughout the following explanations. Except for more details, the most important difference between Algorithm 3 and its simplified version, Algorithm 2, is that the search process to find a new peak per cycle is conducted in a dynamic fashion by introducing a new parameter, ω , that we call peak finder patience counter. The flowchart in Fig. 6 does not go down into the smallest details of every single line in Algorithm 3 yet it reflects on the most important steps to clarify the process. As can be seen in Fig. 6, there are three components: a) initialization (a one-off process), b) label map aggregation (corresponding to Algorithm 1), and c) the main body of LoAd for semantic segmentation (corresponding to Algorithm 3). The process starts from initialization depicted on the top left (part a), which corresponds to the preamble of Algorithm 3. Provided a starting model, the cycles of LoAd can start and iterate between its main body (part c) and its label map aggregation module (part b).

Let us delve deeper into this process by zooming into Algorithm 3. Lines 3 to 35 outline what happens in a single cycle of LoAd. A cycle starts by initializing the divergence patience counter $\gamma \in [0, \dots, \Gamma]$ and the peak finder patience counter $\omega \in [0, \dots, \Omega]$. At the beginning of every cycle, we mark the very initial model performance (in mIoU) as μ^0 which will only be used in line 26 to decide if throughout the cycle we actually found a new model (a new peak in the convergence graph) that is better than the very initial model of the cycle in mIoU sense. Lines 7 to 24 embody the main while loop of the cycle that keeps training the adversarial network until one of the following conditions is met: 1) the current mIoU (μ) touches the bottom line we defined for downward/divergence trend ($\mu^s - \beta_l < \mu$) or γ meets its limit in the number of iterations. Inside this while loop, we watch for finding a new peak (model) in lines 10 to 22, and such a peak is only valid if the current mIoU goes beyond the starting mIoU plus a minimum increment ($\mu > \mu^s + \beta_u$). We came to understand by extensive experimentation that if the starting model (g^s with mIoU μ^s) is kept unchanged in this while loop (e.g., kept as μ^0 as in line 4), and thus, we select a peak based on a static peak finder patience counter ω , we can prematurely kill an upward trend leading to a higher peak. This is the rationale behind the dynamic peak finding process in which we dynamically update the starting model (g^s, μ^s) in lines 16 and 17. To do so, every time we reach the end of a peak finding process (ω reaches Ω), if the mIoU is beyond the current starting model mIoU by at least β_u in mIoU sense, we reset both γ and ω and allow this upward trend to continue and keep updating the best model. This is delineated in lines 15 to 20.

At the end of this inner while loop (lines 7 to 24), we are expected to mark one or two models: an ending model and possibly a new peak. The ending model of the cycle g^e (line 25) will be passed to the label map aggregation module regardless of whether we find a new peak or not. In case the dynamic peak finding process discovers a new peak that is better than the initial model of the cycle ($\mu^* > \mu^0$), then we pass both the new peak model g^* and the ending model g^e to our label map aggregation module. Lines 29 and 32 highlight the two ways in which the label map aggregation module can be invoked, with and without a new peak found. Based on that the map aggregation buffer \mathcal{B} will be updated at the end of each cycle. The containment of the updated buffer will be concatenated with the full training dataset ($\mathcal{D}_t \cup \mathcal{B}$) and will be used to retrain the discriminator (line 35). As discussed in Section 2, we do not follow a standard GDA approach and every time train the discriminator with this dynamically updated dataset until a sufficient accuracy is reached. Lastly, a new peak serves as a new starting model based on which counting the cycles will be restarted (lines 27, 28 and 30). On the other hand, if no new peak is found, we go back to where we started and continue (lines 32 and 33) hoping for finding a new peak in the next cycle. We fully stop the algorithm if we run Ψ cycles and a new peak is not found. This process is also sketched in Fig. 6.

Algorithm 3: LoAd for Semantic Segmentation - Detailed Version

Initialize: $\psi = 0$, $g^s = g_0$, $\mathcal{B} = g^s(\mathcal{X}_t)$ **Input:** maximum cycle: Ψ , maximum divergence: Γ , maximum peak finder: Ω , β_l , β_u

```
1  $\mu^s, \mu, \mu^* \leftarrow \text{Evaluate mIoU}$ 
2  $\text{Train Discriminator}(\mathcal{D}_t \cup \mathcal{B})$ 
3 while  $\psi < \Psi$  do
4   keep the very first starting point:  $\mu^0 \leftarrow \mu^s$ 
5   start a divergence patience counter:  $\gamma \leftarrow 0$ 
6   start a peak finder patience counter:  $\omega \leftarrow 0$ 
7   while  $\mu^s - \beta_l < \mu$  and  $\gamma < \Gamma$  do
8     update the model:  $g \leftarrow \text{Train Adversarial}$ 
9      $\mu \leftarrow \text{Evaluate mIoU}$ 
10    if  $\mu > \mu^s + \beta_u$  then
11      if new peak is found:  $\mu > \mu^*$  then
12        update best performance:  $\mu^* \leftarrow \mu$ 
13        update best model:  $g^* \leftarrow g$ 
14      end
15      if  $\omega > \Omega$  then
16        update starting performance:  $\mu^s \leftarrow \mu$ 
17        update starting model:  $g^s \leftarrow g$ 
18        reset peak finder counter:  $\omega \leftarrow 0$ 
19        reset divergence counter:  $\gamma \leftarrow 0$ 
20      end
21       $\omega \leftarrow \omega + 1$ 
22    end
23     $\gamma \leftarrow \gamma + 1$ 
24  end
25   $g^e \leftarrow \text{keep last model of the cycle}$ 
26  if best peak is better than very first start:  $\mu^* > \mu^0$  then
27    set best model as start model:  $g^s \leftarrow g^*$ 
28    set best mIoU as start mIoU:  $\mu^s \leftarrow \mu^*$ 
29     $\mathcal{B} \leftarrow \text{Lookahead Map Aggregation}(g^*, g^e, \mathcal{X})$ 
30    reset cycle counter  $\psi \leftarrow 0$ 
31  else
32     $\mathcal{B} \leftarrow \text{Lookahead Map Aggregation}(0, g^e, \mathcal{X})$ 
33    start a new cycle  $\psi \leftarrow \psi + 1$ 
34  end
35   $\text{Train Discriminator}(\mathcal{D}_t \cup \mathcal{B})$ 
36 end
```

D Ablation Study

A potential downside of LoAd is that it might be somewhat sensitive to the specific architectures currently being employed even though our preliminary results with VGG16 as well as a custom designed CNN as discriminator did not result in performance degradation. Main question here is focused more on the impact of changing the generator/segmentor model (currently DeepLabv3+). In this section, we already took one step towards addressing this question by changing the backbone of DeepLabv3+. Table 4 summarizes the results of our experiments with a different backbone (MobileNetv2) for the segmentor in comparison with the main backbone used in our previous experimentation (Xception-65). Obviously, a weaker backbone

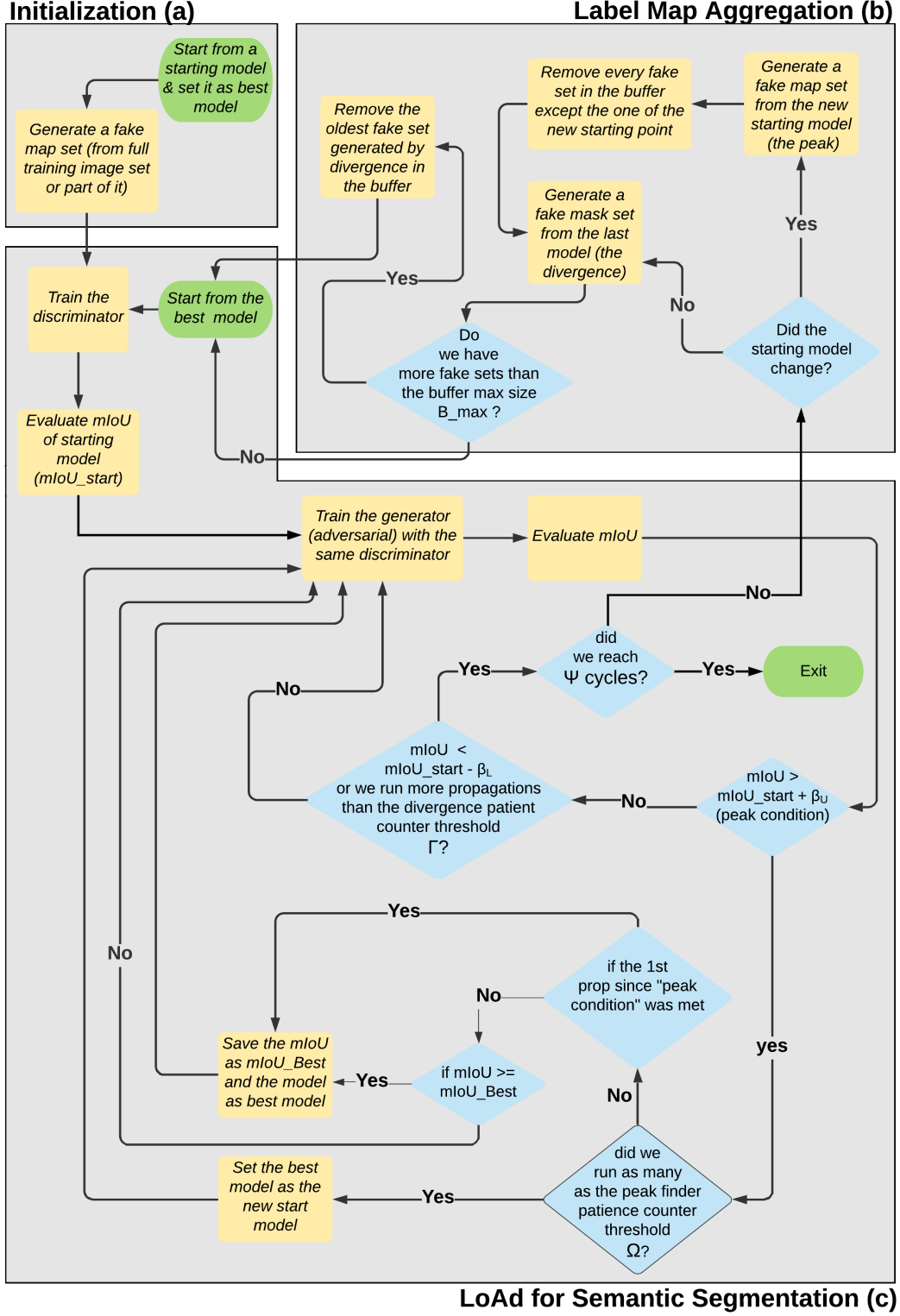


Figure 6: Process flow of LoAd with label map aggregation for semantic segmentation.

Table 4: Impact of generator backbone change for *val* and *test* results of PASCAL VOC 2012.

Method	Gen. backbone	mIoU (<i>val</i>)	mIoU (<i>test</i>)
DLv3+	Xception-65	82.20	76.81
DL3+ & LoAd	Xception-65	82.84	77.39
DLv3+	MobileNetv2	75.32	71.45
DL3+ & LoAd	MobileNetv2	75.70	71.74

Table 5: Influence of hyperparameter change on LoAd for *val* results of PASCAL VOC 2012. The backbone model is Xception-65 which is employed in most of our experimentation.

Method	$\beta_l(\%)$	B_{\max}	mIoU (<i>val</i>)
DLv3+	-	-	82.20
DL3+ & LoAd	5	3	82.84
DL3+ & LoAd	10	3	82.80
DL3+ & LoAd	5	4	82.46

(MobileNetv2) results in performance drop for both baseline and boosted model with LoAd on *validation* and *test* datasets. Nevertheless, what remains consistent is the improvement of DeepLabv3+ & LoAd over the baseline, even though the improvement is a bit less pronounced for both *validation* and *test* datasets. Check out anonymized *test* results for baseline DeepLabv3+⁵ and proposed method DeepLabv3+ & LoAd⁶ with MobileNetv2 backbone on PASCAL VOC server.

Another angle to investigate is the impact of hyperparameter change on the performance of DeepLabv3+&LoAd. We limited this experiment to selecting the following two hyperparameters (one from the main body of LoAd and the other from the map aggregation module): the lower-bound based on which a divergence is marked, β_l , and the maximum set size of the map aggregation buffer, B_{\max} . The results are extracted with our main choice of backbone (Xception-65) and summarized in Table 5. As can be seen, lowering β_l to 10% (in mIoU) does not seem to have a considerable impact on the overall mIoU, whereas increasing the maximum set size of the buffer results in degradation in performance of DeepLabv3+ & LoAd in comparison with the best setting $\beta_l = 5\%$ and $B_{\max} = 3$. This could potentially be due to the fact that we only generate and aggregate “fake” label map datasets, keeping only one ground truth label map set. This can be a source of imbalance if too many of these sets are aggregated. To alleviate this issue, besides weighting the discriminator loss as discussed in Section 4, we introduced the maximum set size B_{\max} . A possible remedy for this issue can be generating fake label maps (using ending and peak models at the end of each cycle) only over a subset of training image set, e.g., images that have been seen by the corresponding model (peak or ending) up to that stage of training. As discussed briefly in Section 6, this can already be accommodated in the label map aggregation module of LoAd in Algorithm 1.

E More Qualitative Results

In this section, we provide further evidence of the impact of LoAd in boosting the performance of the baseline DeepLabv3+ model. As can be seen in Fig. 7, the top two rows demonstrate more examples of how “sofa” and “dining table” are segmented with considerably better consistency and continuity. The third row illustrates the continuity in segmenting “bird” foot. The fourth row shows how LoAd outperforms baseline DeepLabv3+ in detecting the “bird” in the cluttered scene, and manages to (a good extent) resolve the confusion of tree trunk with another bird in the scene. Last row, depicts cleaner edges at the bottom and around the “boat”.

⁵DLv3+ (MobileNetv2): <http://host.robots.ox.ac.uk:8080/anonymous/9ZCKBC.html>

⁶DLv3+&LoAd (MobileNetv2): <http://host.robots.ox.ac.uk:8080/anonymous/LMCYVC.html>

To further consolidate the qualitative dominance of DeepLabv3+ & LoAd compared to the baseline, we provide eight new examples in Figs. 8 and 9 (in the same fashion as in Fig. 5) where gradual impact of LoAd on the performance of the baseline throughout its cycles (ending up with divergence or leading to finding new peaks) is at the center of attention. The first example (top two rows) in Fig. 8 is a prime example of how a complete instance of “sofa” is missed by the baseline DeepLabv3+ (b), whereas LoAd manages to almost completely recover it (h). The second example (next two rows) reiterates the same message, offering much better consistency compared to the baseline. The third example (third two rows) poses a challenging scenario where a “boat” and an “aeroplane” are confused due to perspective and texture complexity. LoAd (h) shows a considerable improvement in resolving this confusion. Last example in this figure depicts how the missing bottom part of the bottle is recovered owing to label map aggregation. The same story continues in Fig. 9. Top two examples highlight how LoAd helps the baseline DeepLabv3+ to infill the gaps and missing pieces in segmenting a “dinning table”. Last two examples (last four rows) in the figure yet again demonstrate how class confusion (“sofa” vs. “chair”) in comparison with the baseline.

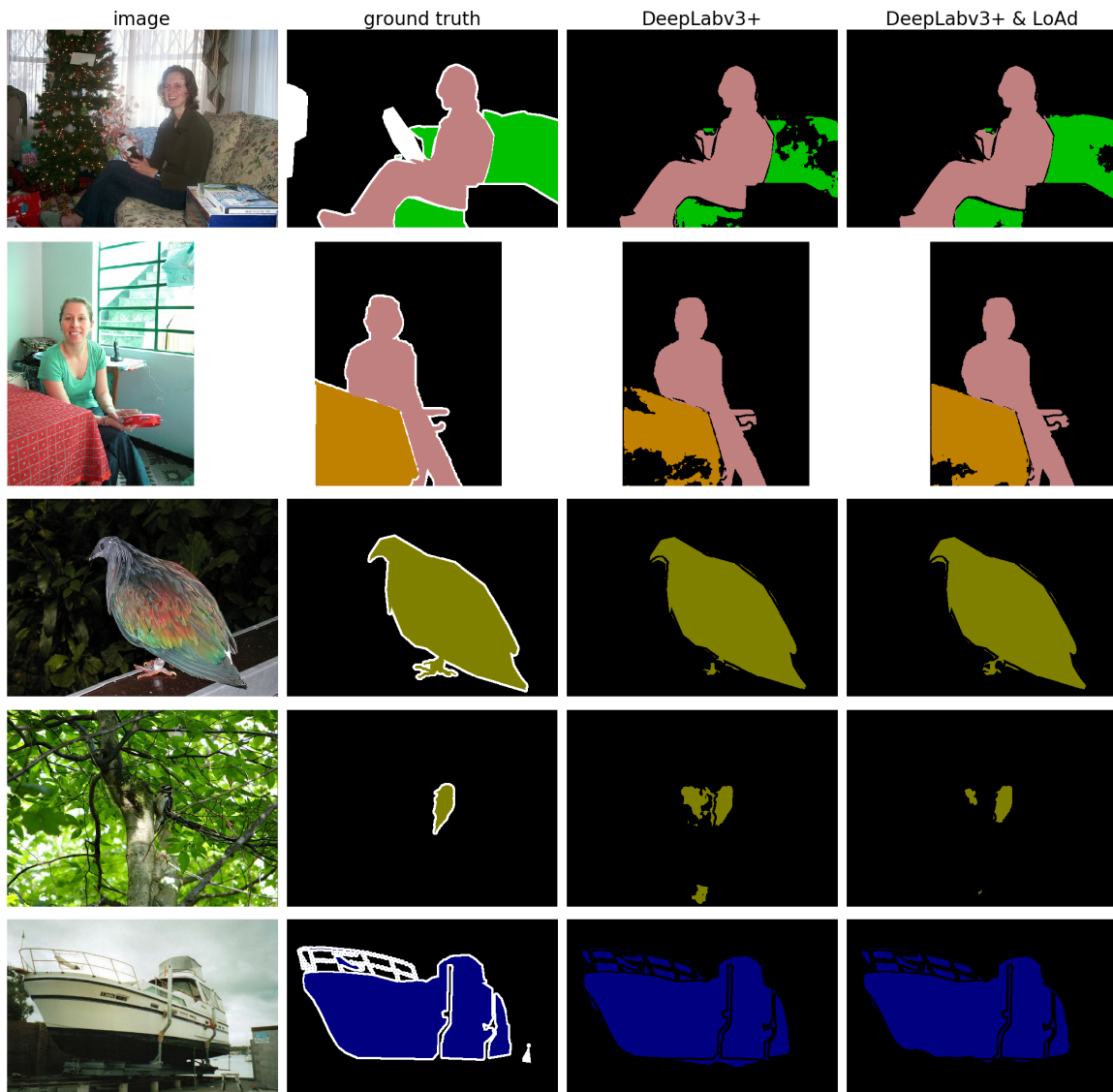


Figure 7: Selected qualitative results on PASCAL VOC 2012. Best view in color with 300% zoom.

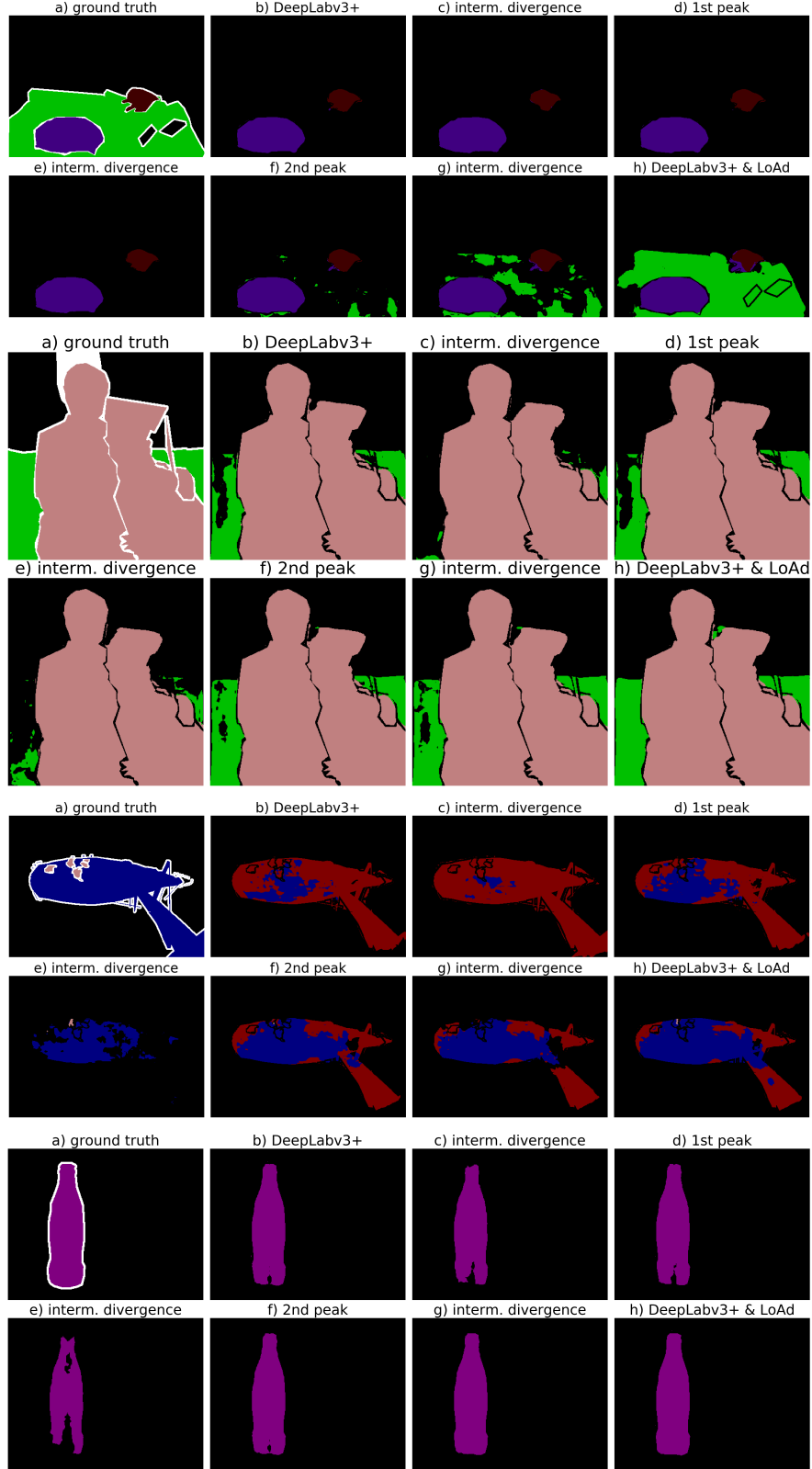


Figure 8: This illustrates how LoAd benefits from label map aggregation throughout its convergence process to boost the performance of the baseline DeepLabv3+. Best view in color with 300% zoom.

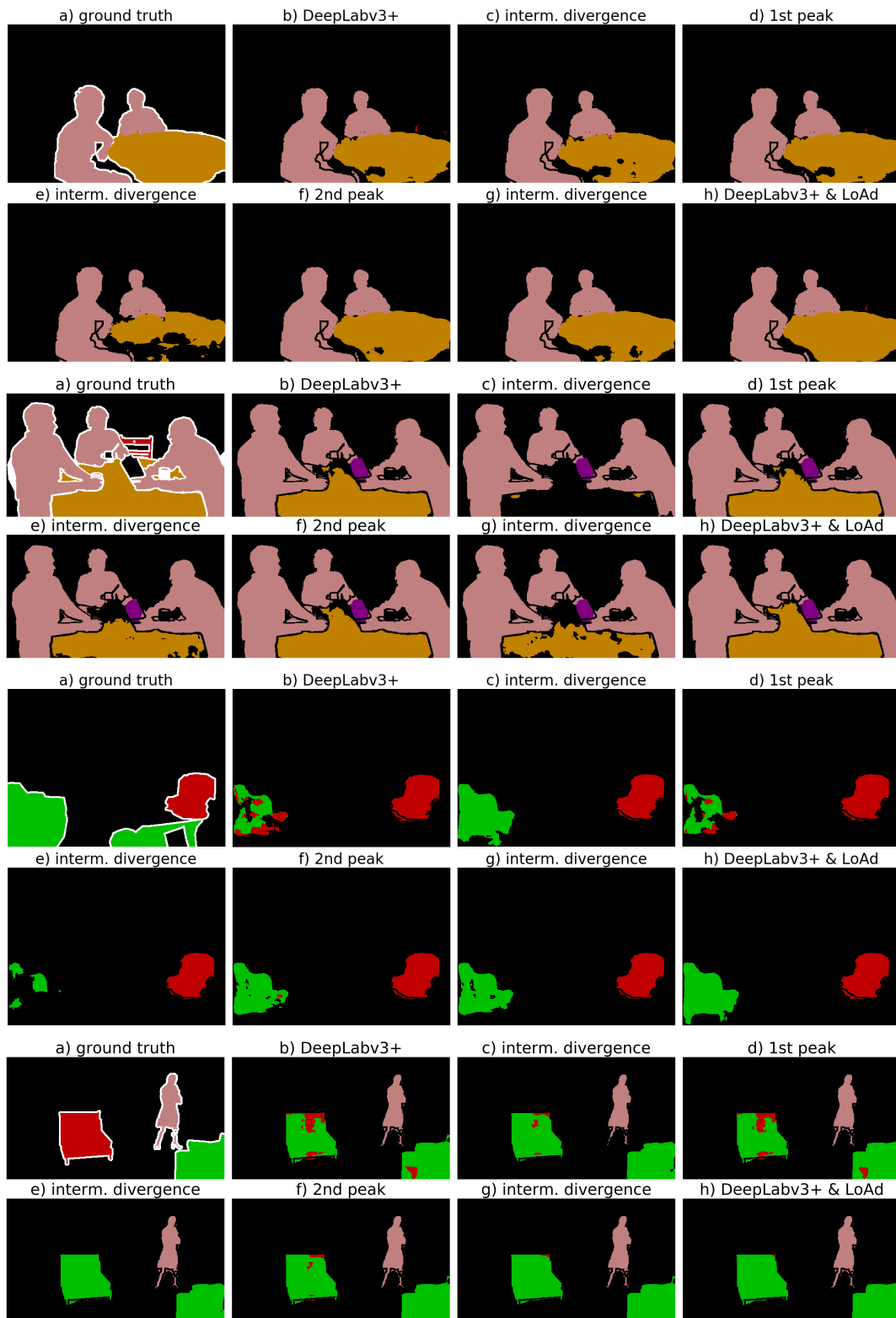


Figure 9: This illustrates how LoAd benefits from label map aggregation throughout its convergence process to boost the performance of the baseline DeepLabv3+. Best view in color with 300% zoom.